Study of Film Formation on Grooved Tools in an Atomization-Based Cutting Fluid Delivery System for Titanium Machining

Devashish R. Kulkarni
Department of Mechanical Science and Engineering,
University of Illinois,
Urbana, IL 61801

Soham S. Mujumdar
Department of Mechanical Science and Engineering,
University of Illinois,
Urbana, IL 61801

Shiv G. Kapoor[1]
Professor
Department of Mechanical Science and Engineering,
University of Illinois,
Urbana, IL 61801
e-mail: sgkapoor@illinois.edu

The purpose of this paper is to study the effect of cutting tool surface geometry and the atomization-based cutting fluid (ACF) spray parameters on the characteristics of the thin film formed in an ACF delivery system. A computational model is developed using three submodels that are used to predict the carrier gas flow, droplet trajectories and the film formation, respectively. The model is validated through film thickness measurements using a laser displacement sensor. Turning inserts with chip-breaking grooves along with a conventional flat insert are used to study the effect of cutting tool surface geometry on the model-predicted film characteristics, including film thickness and velocity. Machining experiments are also conducted to investigate the effect of film characteristics on the machining performance in terms of tool wear, which show that the tool wear is minimum at a certain desired film thickness value and large film velocity value. Carrier gas pressure and cutting fluid flow rate are also varied to study the effect of ACF spray parameters on the film characteristics. Increase in the fluid flow results in increase in both film thickness and velocity, while an increase in the gas pressure results in the reduction of the film thickness but an increase in the film velocity. [DOI: 10.1115/1.4038892]

1 Introduction

Titanium alloys are difficult to machine materials due to their poor thermal conductivity, high affinity to tool materials at cutting temperatures, and production of thin chips during machining [1]. Heat generated in the tool-chip contact region is not readily dissipated, leading to a shortened tool life. Various cooling methods have been studied for titanium machining including high pressure coolant application [2,3], minimum quantity lubrication [4], and recently, the atomization-based cutting fluid (ACF) delivery system to improve upon the cooling and lubrication provided by conventional flood cooling. In the ACF system, the impingement of atomized droplets of the cutting fluid on the tool surface results in the formation of a thin liquid film that penetrates the narrow tool-chip contact region and improves tool life [5]. The characteristics of this thin film such as the film thickness and velocity influence the effectiveness of the ACF system [6] and are dependent on a large number of parameters including cutting fluid properties, spray parameters, i.e., gas pressure, fluid flow rate, spray distance and spray angle, and the cutting tool surface geometry. Therefore, it is imperative to carry out a systematic study of the effect of these parameters on the film formation and associated film characteristics in order to improve the effectiveness of the ACF system in titanium machining.

The concept of ACF system for cutting fluid delivery is relatively new [7] and many experimental as well as modeling studies have been carried out by researchers in recent years to evaluate its effectiveness for various machining operations [5,7,8]. One of the first experimental study was conducted by Nath et al. [5], which showed that the machining performance, including tool-life and surface finish, during titanium turning operation was affected by the ACF parameters. A similar investigation was conducted by Ganguli and Kapoor [8] to establish the effect of ACF spray parameters on the machining performance in titanium milling. However, such experimental efforts are often inadequate in obtaining a quantitative understanding of the effect of all parameters that affect the film formation. Furthermore, the experiments fail to bring forth a clear understanding of the underlying mechanism of the film formation and its penetration in the tool-chip interface. A few efforts have also been made to study the film formation in the ACF system using theoretical modeling. Ghai [7] developed an energy-based approach to predict the spreading behavior of a droplet impinging on a rotating surface for micromachining with an ACF system. However, the dynamics of a single droplet impingement is insufficient to describe the formation of a continuous moving film with the ACF system for a machining operation. Hoyne et al. [6] developed a numerical model using boundary layer approximations of the Navier–Stokes equations to predict the thickness of the thin liquid film formed on a flat surface. However, this model leaves much scope for improvement as it fails to consider the geometry of the spray nozzles that is essential for estimating the droplet trajectories in the carrier gas flow.

Besides the ACF spray parameters, the cutting tool surface geometry (i.e., features such as flute geometry and clearance angles on a milling tool, and chip-breaker grooves on a turning tool) could also significantly affect the film formation in the ACF system. Friedrich et al. [9] studied the film formation on a surface with a sharp corner and found that the dynamics of the film formation due to the sharp corner are different from those on a flat surface. Baxter et al. [10] investigated thin film flows over and around obstacles and found that the film flow depends on the size and shape of the obstacle considered. In addition, features like curvature of the surface are also known to alter the liquid droplet impingement and film flow characteristics [8]. Hence, cutting tools with geometries such as chip-breaking grooves that are used to improve the chip breaking capabilities of the tool could affect the film characteristics due to their specific surface features that alter the flow path of the liquid film.

[1]Corresponding author.

Manuscript received June 28, 2017; final manuscript received December 6, 2017; published online February 12, 2018. Assoc. Editor: Radu Pavel.

The objective of this paper is to study the formation and the influence of the associated film characteristics on the machining of titanium alloys with grooved tools and the ACF system. A numerical modeling approach is used to predict the film characteristics. The system geometry and the spray parameters are used to predict the droplet paths, which are further used to calculate the film thickness and the film velocity. Validation of the numerical model is provided by experimental measurements of film thickness using a laser displacement sensor. Effect of the film characteristics on the machining performance is studied by conducting machining experiments.

The rest of this paper is organized as follows: Section 2 describes formulation of the numerical model used to predict the film formation in an ACF system. Section 3 describes model evaluation, setup for validation experiments, and comparison of the model predictions with the experimental results. Section 4 discusses model predictions of the effects of cutting tool surface geometry on the film characteristics. Finally, conclusions of this study are presented in Sec. 5.

2 Model Formulation

In an ACF system, a thin, moving film of the cutting fluid is delivered at the tool-chip interface [5] as shown in Fig. 1. An ultrasonic atomizer is used to generate a spray of atomized droplets of the cutting fluid, which is impinged onto the surface of the cutting insert to form a thin film. This thin film penetrates the tool-chip interface and provides cooling and lubrication that has been shown to improve the machining performance during a machining operation [5,11,12]. Formation of the cutting fluid film in the ACF system is governed by the droplet-surface interaction and the physical properties of the cutting fluid [6,7]. Therefore, features like chip-breaking grooves in the geometry of the impinged surface play a critical role in the effectiveness of the ACF system during a machining operation. The characteristics of the fluid film including film thickness and velocity profile are also affected by the ACF spray parameters such as fluid flow rate, gas pressure, spray distance, and spray angle (refer to Fig. 1). Recently, Nath et al. [5] have shown that, with the use of the ACF system, the tool-life in turning of titanium alloy can be improved by 50% when compared with the use of conventional flood cooling. Furthermore, the ACF system is known to provide desirable features like low power input for the atomizer, no requirement for the pumping of high volume flow rates of the cutting fluid, and usage of very low volumes of cutting fluid, making it environment friendly.

Figure 2 shows a schematic of the modeling approach adopted in this paper. The approach is similar to the one used by Pattabhiraman et al. [13] in describing dielectric film formation in spray electrical discharge machining. Three different models, namely, the carrier gas model, the discrete phase model (DPM), and the Eulerian wall film model (EWF), are used to simulate ACF spray and the resulting fluid film formation on a cutting tool. The carrier gas model is used to model flow of the carrier gas throughout the domain using the equations of conservation of mass and momentum. The DPM is used to model the movement of atomized droplets of a cutting fluid in the carrier gas flow using the Euler–Lagrange approach. The carrier gas is treated as a continuum by solving the Navier–Stokes equations, while the dispersed phase (atomized droplets) is modeled by tracking a large number of droplets through the calculated gas flow field. The dispersed phase can exchange momentum, mass, and energy with the fluid phase [14]. The trajectory of a discrete phase particle (or droplet or bubble) is predicted by integrating the force balance on the droplets, which is written in a Lagrangian reference frame. Finally, the EWF model is used to study the film formation on the surface of the cutting insert.

The model also includes the nozzle geometry including the nozzle walls as well as the chip-breaker geometry of the spray-impinged cutting tool (both the flat- and the grooved-type turning insert). In addition, the droplet injection parameters at the atomizer outlet that serve as an input to the DPM are chosen from experimental measurements in order to improve the prediction of droplet trajectories. Loss of cutting fluid due to impingement on the nozzle walls is also considered in the model.

The physical properties of the cutting fluid and the surface geometry of the cutting tool on which the cutting fluid film is formed act as inputs to the Eulerian wall film model and significantly influence the formation and characteristics of the fluid film. Specifically, the chip-breaker geometry of the impinged surface (i.e., the turning insert in this case) affects the boundary conditions for the gas and fluid flow, while the physical properties of the cutting fluid appear in the mass and momentum conservation equations. The nozzle geometry and the ACF spray parameters act as inputs to the carrier gas model that predicts the carrier gas velocity profile. The specific ACF spray parameters that are taken into consideration in this model are the fluid flow rate, spray distance, spray angle, and the gas pressure. Using these three models, i.e., carrier gas model, discrete phase model, and the Eulerian wall

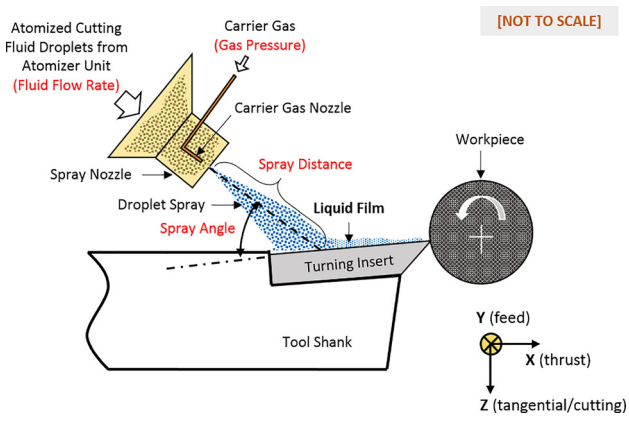

Fig. 1 Schematic of the ACF system in a turning setup showing ACF spray parameters, i.e., fluid flow rate, gas pressure, spray distance, and spray angle

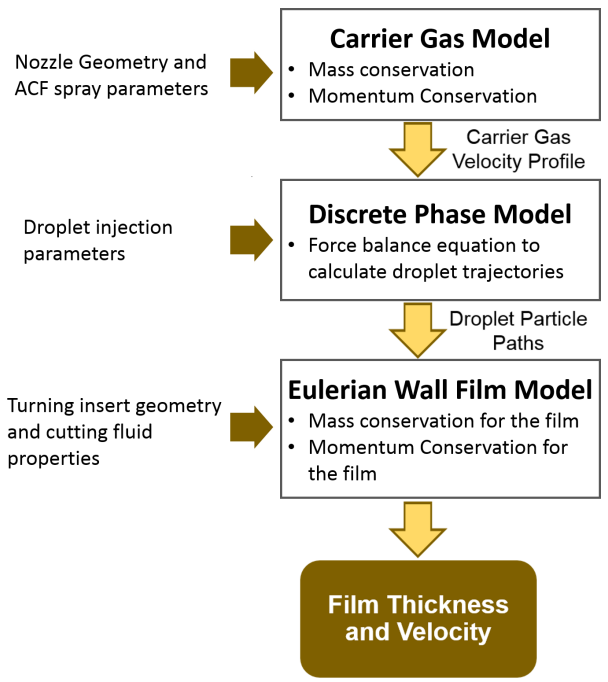

Fig. 2 Schematic of the ACF film formation modeling approach

film model, spatial profiles of thickness and velocity of the cutting fluid film formed by the ACF system on the cutting tool can be obtained. Descriptions of each of these models along with the governing equations are given in rest of the section.

The carrier gas model uses equations of conservation of mass and momentum to model flow of the carrier gas through the computational domain. The carrier gas is treated as a steady, compressible fluid. The mass conservation equation is given as [14]

$$\frac{\partial \rho}{\partial t} + \nabla.(\rho \mathbf{v}) = S_m \tag{1}$$

where ρ, t, $\mathbf{v}$, and S_m are the fluid density, time, fluid velocity, and mass source term, respectively. The momentum conservation equation is given as [14]

$$\frac{\partial(\rho \mathbf{v})}{\partial t} + \nabla.(\rho \mathbf{v}\mathbf{v}) = -\nabla p + \nabla.(\bar{\bar{\tau}}) + \rho \mathbf{g} + \mathbf{F} \tag{2}$$

where p is the static pressure, $\bar{\bar{\tau}}$ is the stress tensor, $\rho \mathbf{g}$ is the gravitational body force, and $\mathbf{F}$ is the external body force (e.g., that arises from interaction with the dispersed phase). The k–ω shear stress transport turbulence model is employed to model turbulent effects [14].

The DPM uses velocity profile of the carrier gas to determine the trajectory of the atomized cutting fluid droplets. The droplets are generated and introduced into the spray nozzle according to the injection parameters such as droplet diameter, droplet mass, and the fluid flow rate. The trajectory of each droplet is predicted by integrating the force balance on the droplet, which is written in a Lagrangian reference frame. This force balance equates the particle inertia with the forces acting on the particle due to drag and gravity [14]

$$\frac{d\mathbf{u}_p}{dt} = F_D(\mathbf{v} - \mathbf{u}_p) + \frac{\mathbf{g}(\rho_p - \rho)}{\rho_p} + \mathbf{F} \tag{3}$$

where $\mathbf{F}$ is the additional acceleration term accounting for forces like Saffman lift force, virtual mass force, or thermophoretic force. $F_D(\mathbf{v} - \mathbf{u}_p)$ is the drag force per unit particle mass and is given by

$$F_D = \frac{18\mu C_D \mathrm{Re}}{24 \rho_p d_0^2} \tag{4}$$

In Eqs. (3) and (4), $\mathbf{v}$ is the carrier gas velocity, $\mathbf{u}_p$ is the liquid particle velocity, μ is the molecular viscosity of the fluid, ρ is the density of the carrier gas, d_0 is the particle diameter, and Re is the relative Reynolds number. Note that the physical properties of the cutting fluid such as density and viscosity affect the forces on each droplet, and hence, the trajectories of the fluid droplets could be different for cutting fluids with different physical properties.

Using the trajectory of the droplets, both the impingement points and the impingement velocities of the droplets on the cutting tool surface are determined. These droplet impingements are treated as mass and momentum source terms in the governing equations for the EWF model. The magnitudes of these terms are determined by calculating the fraction of the droplet mass that is added to the film, which is a function of the droplet velocities, the physical properties of the fluid, and the instantaneous film thickness at the impingement location [14]. The cutting fluid film is modeled as a two-dimensional thin film. The thin film assumption implies that the thickness of the fluid film is small compared to the radius of curvature of the surface, and therefore, the variation of the film properties across the thickness of the film can be ignored. In addition, the motion of the liquid in a film is allowed only parallel to the surface on which it is formed. The assumption is valid because the film thickness values reported for typical atomized/spray fluid delivery systems [6] are in the order of tens of microns, which is small compared to the curvature of the surface of cutting inserts. The film thickness distribution is obtained by solving equations for mass and momentum conservation for the cutting fluid [14]. The mass conservation equation is given as

$$\frac{\partial h}{\partial t} + \nabla_s[h\mathbf{V}_l] = \frac{\dot{m}_s}{\rho_l} \tag{5}$$

where ρ_l is the liquid density, h is the film height, ∇_s is the surface gradient operator, $\mathbf{V}_l$ is the mean film velocity, and $\dot{m}_s$ is the mass source per unit wall area due to droplet collection, film separation, or other phenomena.

Momentum conservation equation for the film is given as

$$\frac{\partial}{\partial t}(h\mathbf{V}_l) + \nabla_s.(h\mathbf{V}_l\mathbf{V}_l) = -\frac{h\nabla_s P_l}{\rho_l} + \mathbf{g}_\tau h + \frac{3}{2\rho_l}\boldsymbol{\tau}_{fs} - \frac{3\nu_l}{h}\mathbf{V}_l + \frac{\dot{q}}{\rho_l} \tag{6}$$

where $P_l = P_{\mathrm{gas}} - \rho h(\mathbf{n}.\mathbf{g}) - \sigma\nabla_s.(\nabla_s h)$. The terms on the left-hand side of Eq. (6) represent the material derivative of the film momentum. On the right-hand side, the first term includes the forces due to the gas-flow pressure, the gravity component normal to the wall surface and surface tension; the second term represents the effect of gravity in the direction parallel to the film; the third term represents the shear force on the surface of the film due to the gas flow outside the film; the fourth term represents the viscous dissipation in the film; and the last term is associated with droplet collection or separation [14]. Often there is a possibility for a liquid film to separate into droplets at the sharp grooves, edges, or obstacles that may be present on the surface on which it is formed. However, in this particular case, it should be noted that the Weber number, i.e., the ratio of inertial forces on the film to surface tension forces, for the film formed by the ACF system is of the order of 10^2 due to its very small thickness ($\approx$20 μm [6]). As a result, it is assumed that the flowing film does not have enough inertia to be separated into droplets at the sharp grooves/edges of the cutting tool [9] and instead flows along the tool surface as a continuous film.

3 Model Implementation and Experimental Validation

The model described in Sec. 2 is evaluated using ANSYS FLUENT computational solver. The computational domain is shown in Fig. 3. As shown in the figure, the domain is divided into three parts, namely, the nozzle unit, the cutting insert, and the intermediate air. The nozzle unit consists of two coaxial nozzles. Cavities are introduced in the fluid domain in the shape of the nozzle walls. The intermediate air is modeled as a cuboidal domain with cavities in the shape of the nozzle unit and the cutting tool, i.e., a turning insert. The position and the orientation of these cavities are adjusted according to the required spray distance and spray angle. The domain is made large enough so that the gas flow in the domain is not influenced by the boundaries of the domain. The turning insert is modeled as a triangular prism with the cutting edge having a radius of 1/32 in. Additional modifications in the geometry of the domain are made for simulating the film formation on grooved inserts by including the chip-breaker geometry on the surface of the triangular prism. In order to reduce the computational time, only a half of the computational domain is used in the model evaluation by exploiting symmetry boundary condition. The domain is meshed with about 800,000 elements having a maximum size of 3 mm. Spatial variations in properties like film thickness and gas velocity are likely be present over a smaller length scale in regions such as the insert tip and the gas nozzle outlet, respectively, because of the small radius of the insert tip and the small diameter of the gas nozzle outlet. Therefore, a mesh refinement is introduced in these regions.

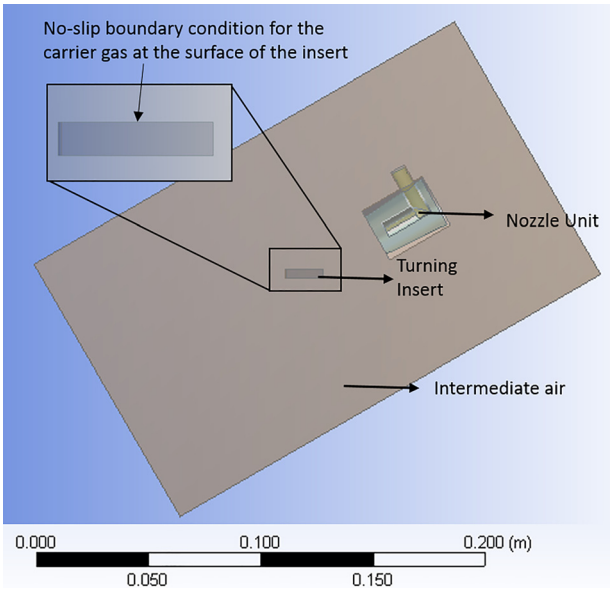

Fig. 3 Computational domain used to evaluate the film formation model

The inlet to the gas nozzle is modeled as a pressure-inlet boundary with the required carrier gas pressure. The outer surfaces of the fluid domain are modeled as pressure-outlet boundaries with atmospheric pressure to represent the quiescent air. No-slip boundary conditions are set on the surface of the turning insert. Different insert geometries can alter the carrier gas flow through the no-slip boundary condition. Cutting fluid droplets are injected at the spray nozzle inlet in a conical spray distribution with a cone angle of 20 deg measured at the outlet of the atomizer experimentally. The physical properties of the liquid droplets are assigned and a uniform droplet diameter of 60 μm is assumed along with the required flow rate. Once the droplets get entrained in the carrier gas flow and get impinged on the insert surface, the surface is allowed to trap the impinging droplets. Mass and momentum of the impinged droplets appear as the source terms in the film mass and momentum equations of the EWF model. Cutting fluid droplets are also allowed to be trapped by the nozzle walls to account for the wasted cutting fluid that flows directly out of the atomizer due to impingement on the inner walls of the spray nozzle. The boundary conditions on the various boundaries of the computational domain are summarized in Table 1. The entire model is simulated for a flow time of 300 ms with a time-step of 0.1 ms.

The model was validated by comparing the experimental measurements of ACF film thickness to the corresponding model predictions. A schematic of the experimental setup used for film thickness measurements is shown in Fig. 4. It consists of a standalone ACF system and a laser displacement sensor. The ACF system includes an ultrasonic atomizer (Model VC5040AT from Sonic and Materials, Inc., Newtown, CT [15]) with a frequency of 40 kHz that can generate atomized cutting fluid droplets with a median diameter of 60 μm. The fluid flow rate at the outlet of the atomizer is 5.9 mL/min. The carrier gas used is air at a pressure of

Table 1 Boundary conditions for the numerical model

Boundary name	Carrier gas BC	DPM (droplet) BC
Domain boundaries	Pressure outlet (atmospheric pressure)	Escape
Gas nozzle inlet	Pressure inlet	Escape
Nozzle walls	No-slip	Trap
Insert surface	No-slip	Trap (EWF model enabled)

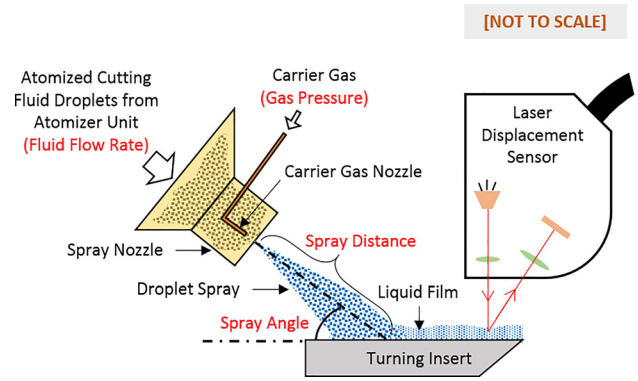

Fig. 4 Schematic of the experimental setup for ACF film thickness measurement using a laser displacement sensor

10 psi. A low pressure and low flow rate was used to facilitate the film thickness measurements, which get difficult at higher pressures due to the large fluctuations in the film thickness caused by the large shear on the film surface due to the high-pressure gas. At high flow rates, there is a possibility for the large number of fluid droplet impinging on the surface of the sensor and blocking the laser beam. The spray angle and the spray distance used are 30 deg and 30 mm, respectively. The impingement point is set at a distance of 14 mm from the cutting edge of the insert so that the maximum area near the cutting edge of the insert falls in the steady zone of the film where measurements can be made [6].

A Keyence LT-9010M laser displacement sensor was used to obtain film thickness measurement at various points on the surface of a flat turning insert as shown in Fig. 5. Here, X represents the distance from the impingement point along the centerline of the tool and Y represents the perpendicular offset distance from the centerline of the insert. The film thickness measurement by the laser sensor involves the detection of the light reflected back to the sensor, which is only possible of surfaces that are almost perpendicular to the laser beam. Hence, only a flat insert was used for the film thickness measurements. The model was evaluated for two different cutting fluids, i.e., 10% S-1001 and de-ionized (DI) water using the same ACF spray parameters used in experiments. Table 2 lists the physical properties of the two fluids used. During the experiments, it was observed that the film thickness value at a given measurement point on the insert surface fluctuates with time due to transient nature of the film and shear instabilities of the fluid. Therefore, film thickness measurements were conducted for

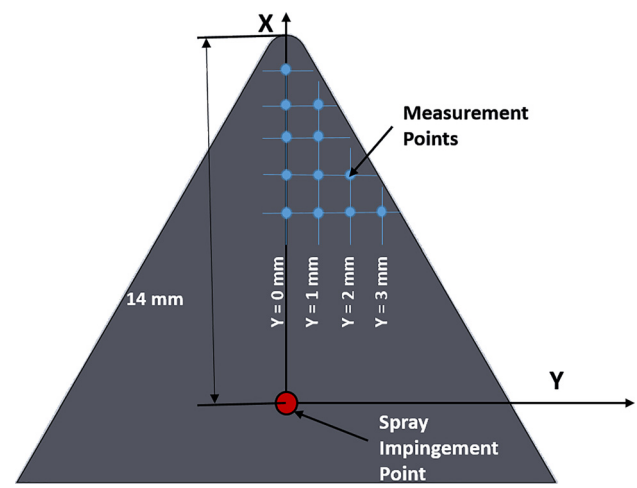

Fig. 5 A schematic showing locations of experimental film thickness measurement points

a period of 30 s and a single time-averaged film thickness value with a standard deviation is obtained at each measurement point.

Figures 6 and 7 show comparison of the experimental time-averaged film thickness values and model-predicted values for S-1001 and DI water, respectively. The experimental error bars are placed at ±standard deviation. From Figs. 6 and 7, it is observed that the model predictions are accurate within one standard deviation of the experimental measurements of the time-averaged film thickness across the surface of the insert for both the cutting fluids. The model also captures the trend of the film thickness with the distance from the impingement point fairly well for both the fluids used. The figures show that the experimental film thickness values remain almost constant with an increasing distance from the impingement point (i.e., along X) in the region where the measurements are made. A similar trend is also found in the model predictions. However, the model predicts a drop in the film thickness as the distance from impingement decreases in the region close to the impingement point where the experimental measurement could not be made due to the obstruction caused to the spray by the laser sensor. However, the low film thickness values near the impingement point were confirmed by the experiments conducted by Hoyne et al. [6]. Note that the experimental measurement for DI water at $Y = 3$ mm is not available as the DI water does not readily spread to the edges of the turning insert due to its high surface tension, thus, making it difficult to obtain a continuous film thickness measurement.

4 Evaluation of the Atomization-Based Cutting Fluid System for Grooved Cutting Inserts

With advances in the cutting tool design, new tool geometries such as turning inserts with chip-breaking grooves are being employed to improve the machining performance by breaking the formed chips and reducing machining forces [16,17]. It has been shown that the surface geometry of the impinged surface could affect the film formation when the ACF system is used [8–10]. Therefore, in order to assess the applicability and effectiveness of the ACF system with grooved turning inserts, the ACF film formation model described in Sec. 2 was used to study the film characteristics, i.e., film thickness and velocity, with two specific geometries as shown in Fig. 8. These specific grooved insert geometries were chosen due to their recommended use by the tool manufacturer [18] for turning of high temperature alloys including titanium alloys. For each insert, the ACF parameters were varied to further understand how the film characteristics vary with the spray parameters for a given chip-breaking geometry. To study how the ACF film characteristics on different insert geometries translate to improvements in the machining performance, turning experiments were also carried out using the same insert and ACF spray parameters as used in the model predictions. Tool flank wear was considered as the measure of machining performance and was correlated with the model predictions of film thickness and film velocity for different tools across a range of ACF spray parameters. Section 4.1 discusses the effect of cutting tool geometry and ACF spray parameters on the film formation using the model followed by Sec. 4.2 that describes experimental investigation of the effect of cutting tool geometry and ACF spray parameters on the machining performance.

4.1 Film Formation on Grooved Inserts. Figures 9 and 10 compare the model-predicted film thickness and film velocity contours, respectively, on three different tool geometries, i.e., a flat insert and two grooved inserts using same ACF spray parameters (fluid flow rate = 15 mL/min, gas pressure = 15 psi, spray distance = 30 mm, and spray angle = 30 deg). It is seen from Fig. 9 that the film thickness values near the cutting edge of the flat insert are around 5–6 μm, while for the grooved inserts, the film thickness near the cutting edge is closer to 10 μm. The elevated surface present on the grooved inserts lowers the gas pressure over the cutting edge and reduces the forces exerted on the fluid film by the carrier gas flow. As a result, the film thickness in the tool-chip contact region near the cutting edge is higher for the grooved insert compared to the flat insert. The specific chip-breaker geometry also affects the distribution of film velocity on the insert surface as seen from Fig. 10. The film velocity near the cutting edge for the grooved inserts is higher in comparison to the flat insert. Therefore, it is expected that, even with the same spray parameters, the ACF system would result in a different machining performance for different cutting tool geometries.

Table 2 Physical properties of the liquids

Fluid	Surface tension	Viscosity	Density
S-1001	0.041 N/m	1.22 mPa s	1003 kg/m^3
Water	0.072 N/m	1.01 mPa s	1000 kg/m^3

As mentioned earlier, the ACF spray parameters also affect the film formation on the impinged surface. In order to study the effect of ACF spray parameters on the film formation for different tool geometries, simulation experiments were conducted using the model for the three turning insert geometries with varying gas pressure and fluid flow rate. Since, during a machining operation, chips move along the rake face of the tool, and the cutting fluid in the tool-chip contact region provides cooling and lubrications [6], it is believed that the machining performance is primarily influenced by the film characteristics in the tool-chip contact region. Hence, the area-averaged film thickness and the area-averaged film velocity in the tool-chip contact region were calculated and used for comparison. The area of the tool-chip contact region considered here is the maximum area of the insert that can be in contact with the chip for a given tool-chip contact length as shown in Fig. 10. Typical tool-chip contact lengths reported for turning of titanium alloys range from 0.5 mm [5] to 3 mm [6] and the tool-chip contact length in this study is assumed to be equal to the depth of cut (1 mm) used in machining experiments. The values of the ACF spray parameters, i.e., gas pressure and fluid flow rate, are chosen from previous studies [8,12].

Figures 11 and 12 present the area-averaged film thickness and area-averaged film velocity, respectively, for varying gas pressure and fluid flow rate for each insert geometry. From the simulations, it is observed that the film thickness and velocity contours become steady after a flow time of ≈300 ms. Therefore, the area-averaging for film thickness and velocity is done at a flow time of 300 ms. It can be seen from the figures that the area-averaged film thickness decreases, while the area-averaged film velocity increases with an increase in the gas pressure for all three insert geometries. At higher gas pressures, the droplets impinge on the surface with a larger momentum that results in the formation of a high velocity film, in general. At higher velocity, the mass flow rate of the liquid exiting the insert surface from the edges is also higher, resulting in a thinner film. However, for the flat and the grooved insert 1, it is seen that the film velocity decreases when the gas pressure is increased from 9 psi to 15 psi. Similarly, for grooved insert 2, the film velocity decreases marginally when pressure increases from 15 psi to 24 psi. One of the reasons for this observation be may be that, for the specific insert geometry, the additional film momentum due to increase in the gas pressure gets transferred to regions on the insert surface that are outside the area considered for averaging. For example, in Fig. 10, the film velocity contour for grooved insert 2 shows large film velocities in regions that are not considered for area-averaging. Another reason could be due to the phenomenon of droplet splashing that counters the momentum of the impinged droplets added to the film. At higher gas pressure, the atomized cutting fluid droplet impact the surface with a higher impact energy, which increases the fraction of impinging droplets being splashed and reduces the fraction being spread to form the film [14]. With a lower fraction of impinging droplets in the spreading regime, the effective momentum that is transferred to the film is reduced resulting in

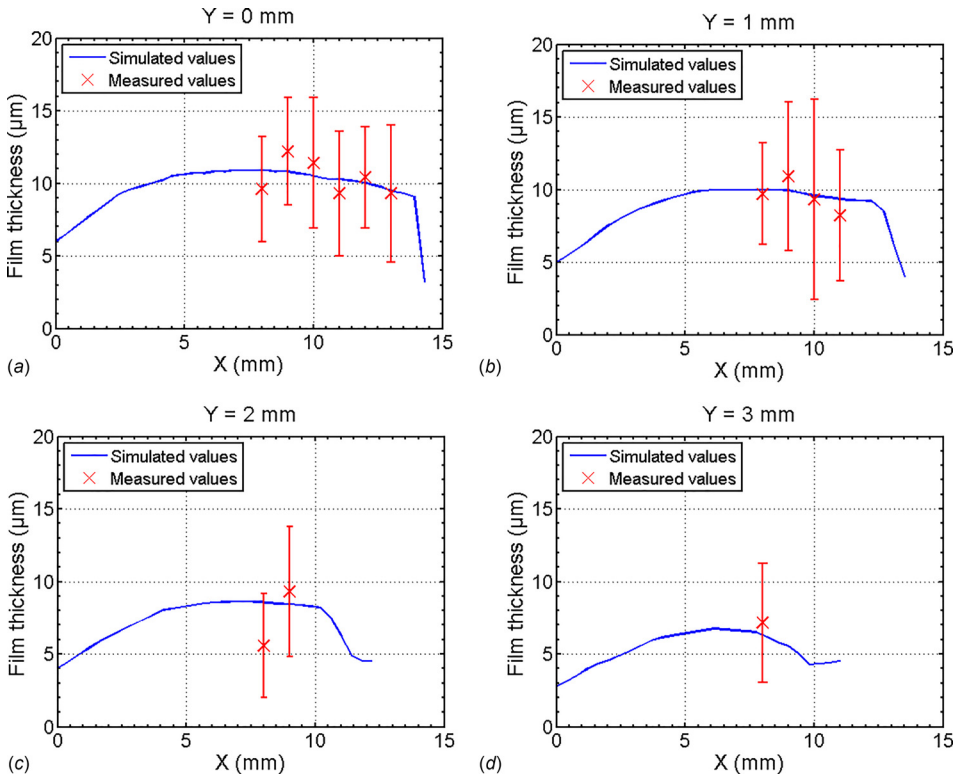

Fig. 6 Comparison of the simulated film thickness values with measurements for S-1001 (*X* is the distance from the impingement point along the centerline of the tool and *Y* is the perpendicular offset distance from the centerline of the insert)

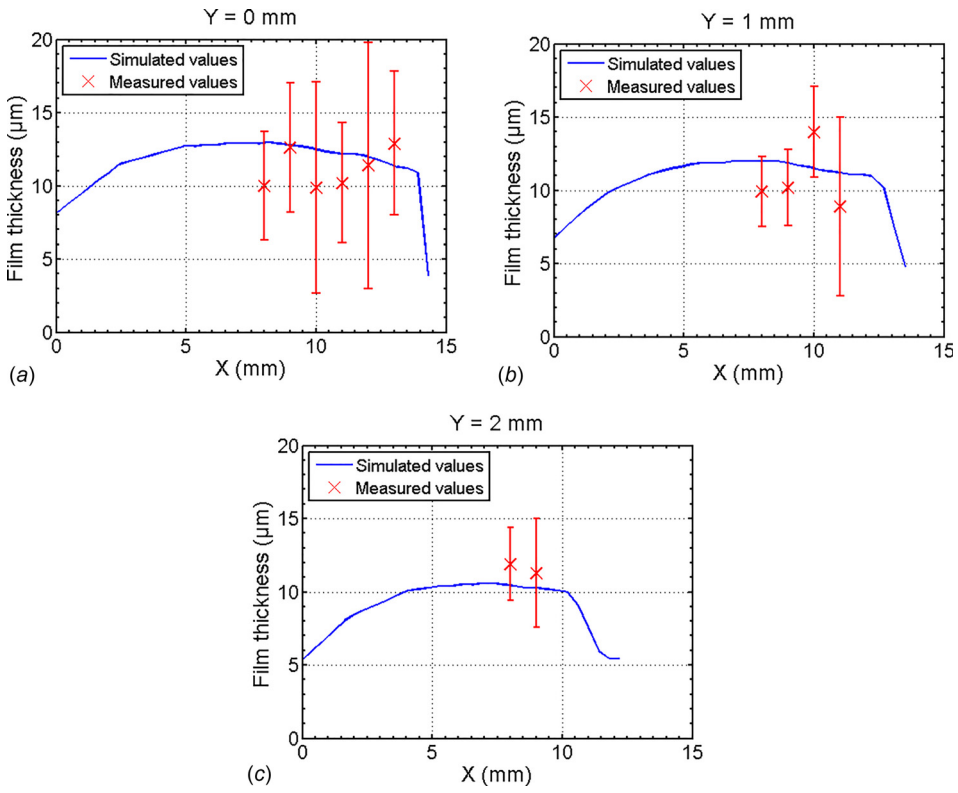

Fig. 7 Comparison of the simulated film thickness values with measurements for DI water (*X* is the distance from the impingement point along the centerline of the tool and *Y* is the perpendicular offset distance from the centerline of the insert)

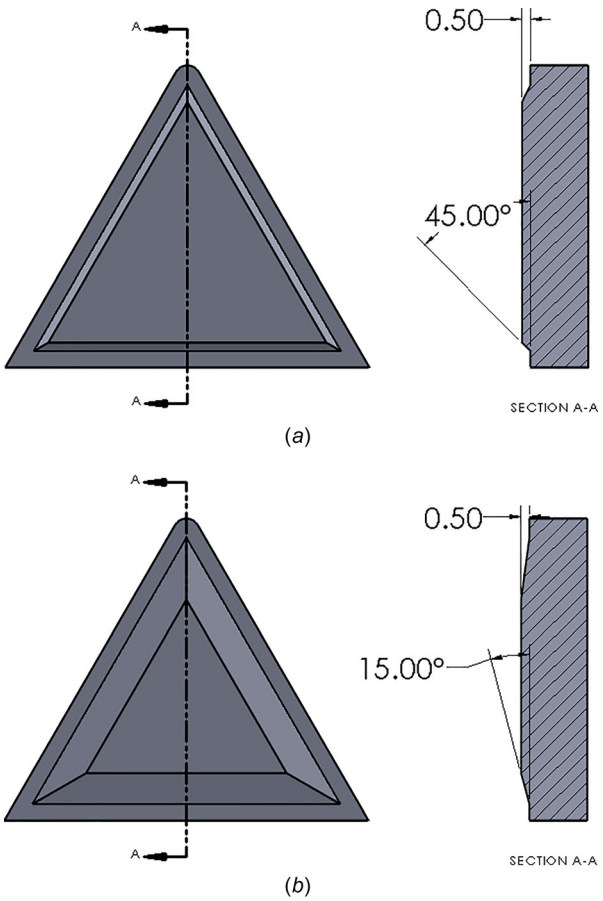

Fig. 8 Grooved turning inserts with chip-breaker geometries: (*a*) grooved insert 1 and (*b*) grooved insert 2

the drop of area-averaged film velocity. However, as the pressure is increased further, the increase in the momentum of the droplets in the spreading regime compensates for the loss of the momentum due to splashing, thus, increasing the film velocity.

Figures 11 and 12 also show that with an increase in the fluid flow rate, both the film thickness and film velocity are found to increase for all three insert geometries. This is because, at a high flow rate, there is a large mass and momentum addition to the film from the impinging droplets, resulting in the formation of thick films with large velocities. The results of area-averaged film thickness and film velocity are tabulated in Table 3. It is also observed from Figs. 11 and 12 that, for the same spray parameters, the area-averaged film thickness and film velocity values are different across the three different insert geometries. Changes in the groove geometry directly affect the film motion by changing the fluid flow path and indirectly affect the film formation by altering the flow of the carrier gas over the cutting inserts. It is seen that for grooved insert 1, the area-averaged film thickness and film velocity values are larger than those for the other two inserts for almost all of the spray parameters considered and a fairly large film thickness is maintained even at high gas pressure. It is believed that the effect of high gas pressure is diminished for grooved insert 1 due to an abrupt change in the form of a sharp corner on the surface of this insert (refer to Fig. 8). Grooved insert 2, on the other hand, has a gradual change in the surface geometry. Therefore, it exhibits area-averaged film thickness and velocity values closer to the flat insert. As a result of higher film thickness, grooved insert 1 is also found to consistently form films with larger velocity compared to the other two inserts. Note that a large film thickness value allows the film to have a large surface velocity due to the presence of a velocity gradient along the film thickness as demonstrated in Fig. 13.

4.2 Machining Performance With Grooved Inserts. Since the cutting tool geometry and the ACF spray parameters are seen to affect the thickness and velocity of the film formed by the ACF system, they would also influence the machining performance because the penetration of the fluid film into the tool-chip contact region depends on these film characteristics. To study the effect of film characteristics on the machining performance using ACF system, tool wear measurements were carried out using turning experiments with the same insert geometries and ACF spray parameters as used to study the film formation (refer to Table 3). A flat insert (Kennametal TPG432 K313 Grade) without any chip-breaker geometry and two grooved inserts with geometries as shown in Fig. 8, i.e., Kennametal TPGF432 KCU10 Grade and Interstate TPMR432 TCN55 Grade, were used. The machining parameters were fixed for all the experimental trials and are listed in Table 4. Turning experiments with dry cutting conditions (no cutting fluid) and with conventional flood delivery of the cutting fluid were also conducted to obtain baseline data. A mixture of 33% CO_2 and air was used as the carrier gas for the ACF as the CO_2 is shown to provide additional cooling to the tool-chip contact region as it cools to a lower temperature when sprayed out of a pressurized tank in comparison to air [5]. A Mori Seiki Frontier L-1 CNC lathe was used for conducting the turning experiments. A machining time of 140 s was chosen because a substantial difference in tool wear was observed between different cutting conditions after 140 s of machining without causing tool failure according to the ISO standard [5]. The impingement point of the ACF spray is set at a distance of 8.4 mm from the cutting edge of the insert so that the tool-chip contact region is in the steady zone

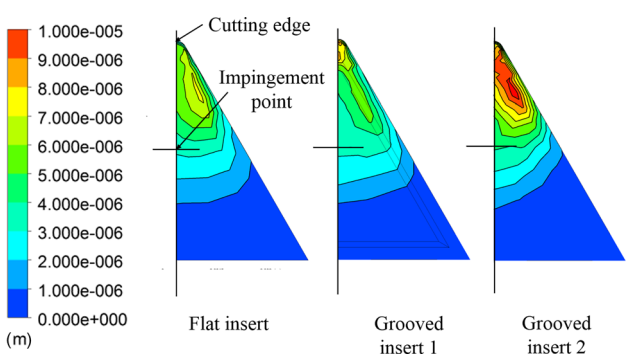

Fig. 9 Film thickness contour comparison between the flat and the grooved inserts (gas pressure = 15 psi, fluid flow rate = 15 mL/min, spray distance = 30 mm, and spray angle = 30 deg)

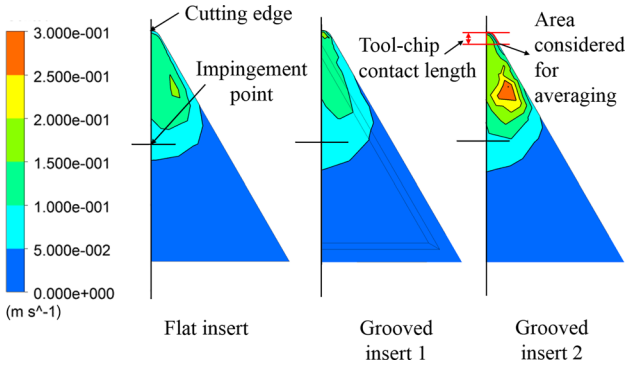

Fig. 10 Film velocity contour comparison between the flat and the grooved inserts (gas pressure = 15 psi, fluid flow rate = 15 mL/min, spray distance = 30 mm, and spray angle = 30 deg)

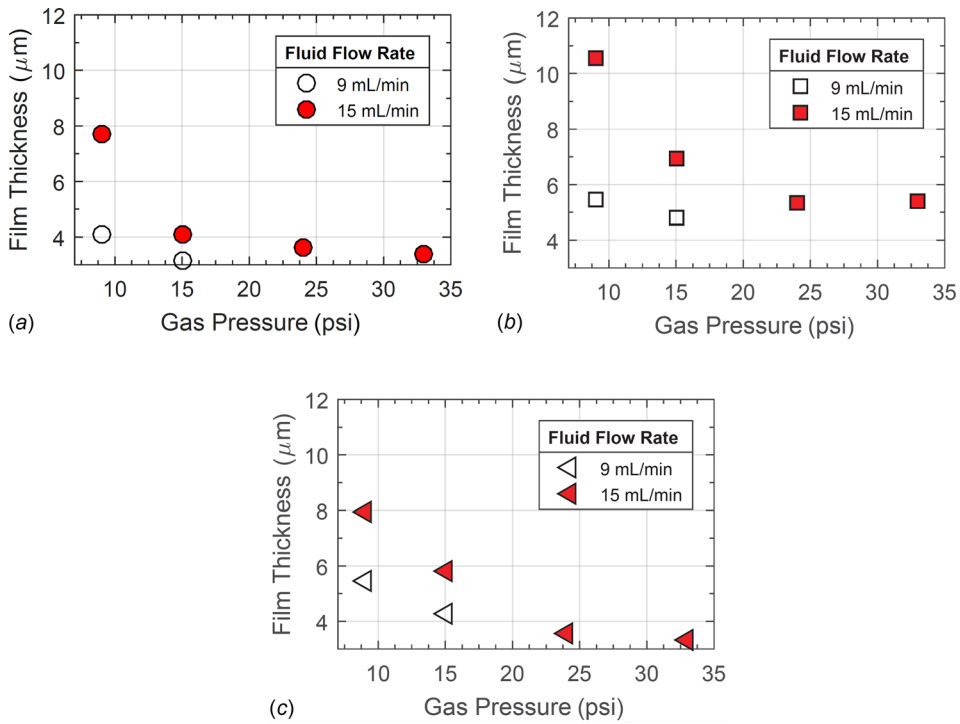

Fig. 11 Model prediction of the effect of ACF spray parameters, i.e., fluid flow rate and the gas pressure on the area-averaged film thickness for various tool geometries: (*a*) flat insert, (*b*) grooved insert 1, and (*c*) grooved insert 2

of the film [6]. Figure 14 shows the setup used for the turning experiments.

Typical flank wear on the turning inserts after dry cutting is shown in Fig. 15. Using the flank wear for dry cutting with a given tool geometry as a reference, a "normalized flank wear" was calculated for each experimental trial as the ratio of flank wear measured for the particular trial to the flank wear for dry cutting. The normalized flank wear can be viewed as a quantification of the improvement of a cooling condition over dry cutting for a given tool geometry, and therefore, allows for the comparison of tool wear across different tool geometries. Model predictions of the area-averaged film thickness and the area-averaged film

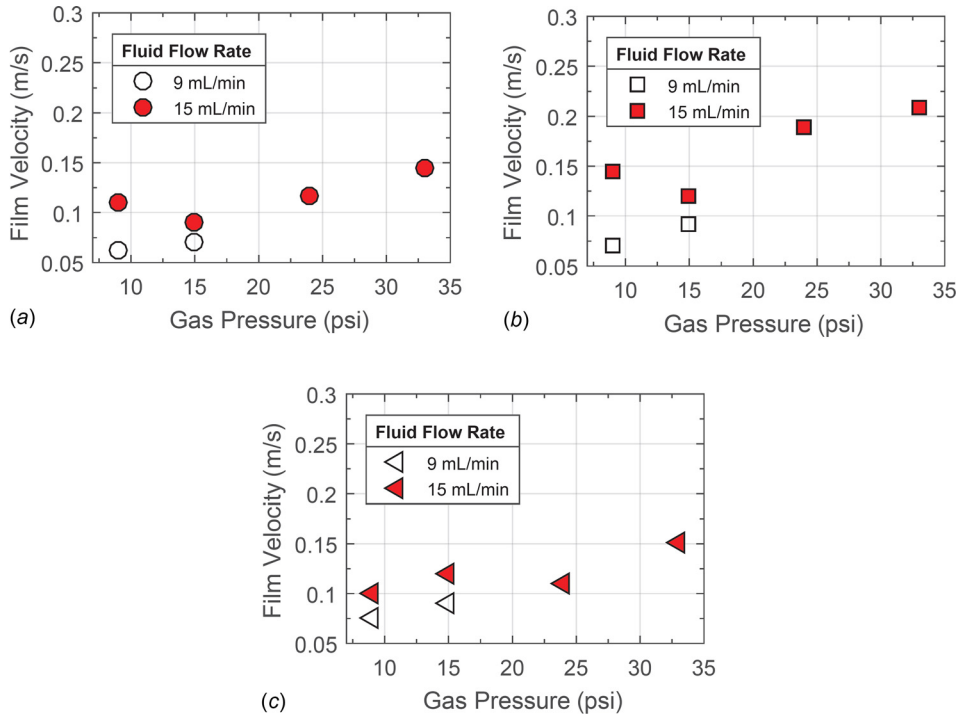

Fig. 12 Model prediction of the effect of ACF spray parameters, i.e., fluid flow rate and the gas pressure on the area-averaged film velocity for various tool geometries: (*a*) flat insert, (*b*) grooved insert 1, and (*c*) grooved insert 2

Table 3 Results of model-predicted film characteristics and experimental measurements of tool wear

Insert type	Cutting condition	Fluid flow rate (mL/min)	Carrier gas pressure (psi)	Area-averaged film thickness (μm)	Area-averaged film velocity (m/s)	Normalized flank wear
Flat	Dry	—	—	—	—	1.00 (0.46 mm)[a]
Flat	Flood	—	—	—	—	0.73
Flat	ACF	9	9	4.09	0.063	0.73
Flat	ACF	9	15	3.15	0.070	0.73
Flat	ACF	15	9	7.72	0.110	0.73
Flat	ACF	15	15	4.10	0.091	0.58
Flat	ACF	15	24	3.60	0.117	0.64
Flat	ACF	15	33	3.40	0.144	0.63
Grooved 1	Dry	—	—	—	—	1.00 (0.61 mm)[a]
Grooved 1	Flood	—	—	—	—	0.83
Grooved 1	ACF	9	9	5.44	0.070	0.81
Grooved 1	ACF	9	15	4.82	0.092	0.62
Grooved 1	ACF	15	9	10.56	0.145	0.69
Grooved 1	ACF	15	15	6.96	0.118	0.53
Grooved 1	ACF	15	24	5.33	0.189	0.40
Grooved 1	ACF	15	33	5.37	0.208	0.41
Grooved 2	Dry	—	—	—	—	1.00 (0.43 mm)[a]
Grooved 2	Flood	—	—	—	—	0.75
Grooved 2	ACF	9	9	5.47	0.076	0.63
Grooved 2	ACF	9	15	4.26	0.090	0.67
Grooved 2	ACF	15	9	7.93	0.099	0.67
Grooved 2	ACF	15	15	5.79	0.120	0.67
Grooved 2	ACF	15	24	3.57	0.110	0.64
Grooved 2	ACF	15	33	3.33	0.151	0.58

[a]Absolute value of flank wear.

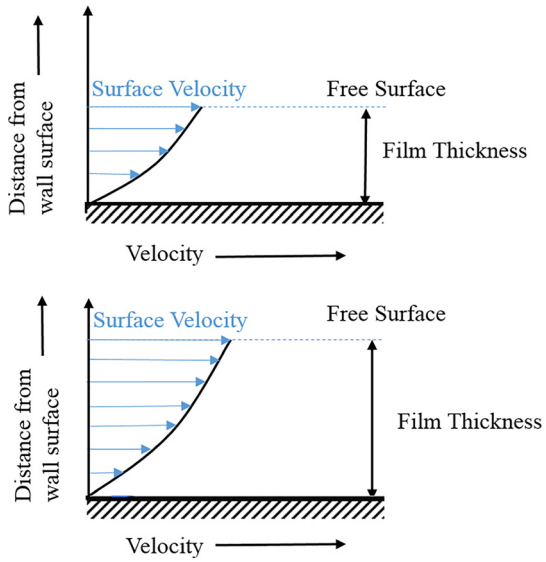

Fig. 13 Velocity gradients in the liquid film

velocity value for each trial were also calculated. Table 3 shows the results of the film characteristics and normalized flank wear obtained from the simulations and machining experiments, respectively. The absolute value of flank wear measured after dry cutting for a given tool geometry is shown in parentheses in the table. All the reported data for wear are the average of two repetitions for each cutting condition.

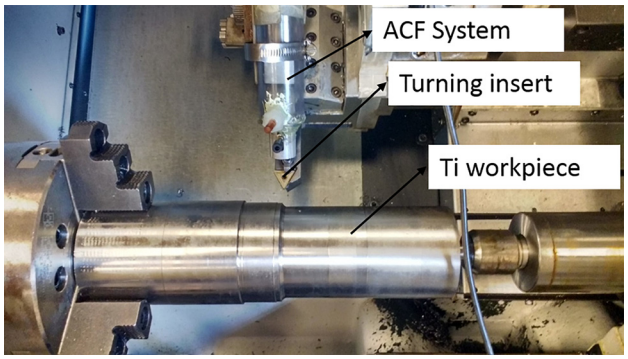

Fig. 14 Setup for turning experiments

A contour plot of normalized flank wear across all three tool geometries as a function of area-averaged film thickness and film velocity is shown in Fig. 16. A linear interpolation scheme is used to estimate the flank wear values between the experimental datapoints. From Fig. 16, it is observed that the normalized flank wear is dependent on both the film thickness and the film velocity. The normalized flank wear shows a minimum value at film thickness of $\approx$5.5 μm and is seen to increase with film thickness that is both larger and smaller than this value. The reason for this trend may be that films having a thickness larger than $\approx$5.5 μm do not effectively penetrate in the tool-chip contact region, while thinner films evaporate before they can provide effective cooling, resulting in film boiling. With increase in the film velocity, however, the normalized flank wear is seen to decrease monotonically as the higher velocity films have a higher heat transfer coefficient that enhances

Table 4 Cutting conditions

Cutting speed	Feed rate	Depth of cut	Spray distance	Spray angle	Carrier gas	Cutting fluid
80 m/min	0.2 mm/rev	1 mm	30 mm	30 deg	33% CO_2 + 67% air	10% S-1001

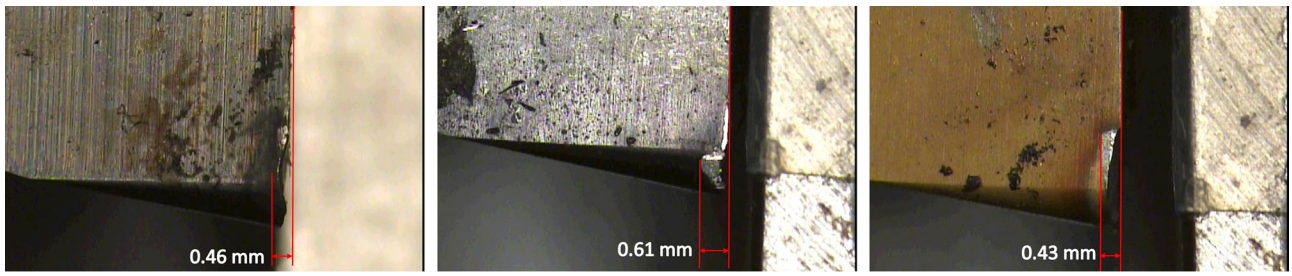

Fig. 15 Tool flank wear in dry cutting: (*a*) flank wear—flat insert, (*b*) flank wear—grooved insert 1, and (*c*): flank wear—grooved insert 2

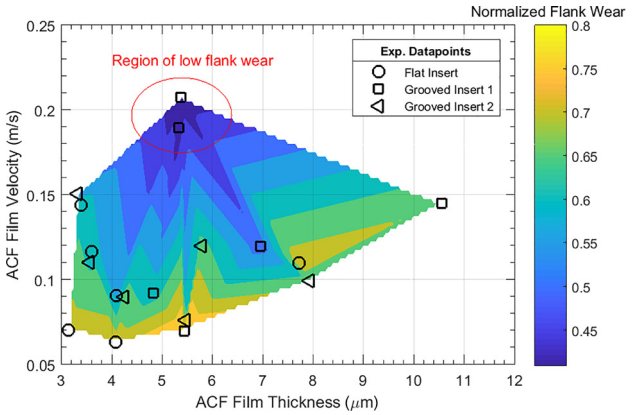

Fig. 16 Normalized tool wear as a function of film thickness and film velocity

the cooling at the tool-chip interface. Higher velocity films also may contribute to the effective penetration of the cutting fluid into the tool-chip contact region and thus provide effective cooling and lubrication.

Note that for grooved insert 1, the film having a high velocity and a large enough thickness results in the minimum normalized flank wear for the range of spray parameters considered (refer to Table 3). For a flat insert, on the other hand, the film thickness reduces significantly at high pressures, which hinders further reduction in tool wear and produces a large value of normalized flank wear. The improvement shown by the ACF system over dry cutting for grooved insert 2 is not as substantial as seen for grooved insert 1 as the film velocity for grooved insert 2 is lower in general as compared to the film velocity for grooved insert 1. The general trend of the effect of the film characteristics on the tool wear is found to be similar for all the three insert geometries considered. Note that the present model does not consider the effect of temperature of the cutting insert on the film characteristics. The high temperature of the cutting insert during a machining operation is expected to alter the film characteristics due to evaporation of the liquid in the film. However, the trends of the film thickness and film velocity with the spray parameters and chip-breaker geometries are expected to be similar.

5 Conclusions

A computational model is developed to study the film formation on grooved tools when machining titanium with the ACF system. The model uses three submodels, i.e., carrier gas model, discrete phase model, and the Eulerian wall film model, that predict carrier gas flow, droplet paths, and liquid film formation, respectively. The model is experimentally validated with two different cutting fluids using film thickness measurements from a laser displacement sensor. The model is then used to study the effect of chip breaking geometries of the turning inserts on the film formation. Machining experiments were also conducted to investigate the effect of film characteristics on the machining performance in titanium turning. The specific conclusions of the research are as follows:

(1) The film formation model is used to predict the film thickness and film velocity on two turning inserts with chip-breaking geometries and on a conventional flat insert. It is seen that the presence of specific chip-breaking grooves on the surface of the insert results in formation of films with higher thickness and velocities when compared to the films on a flat insert.
(2) ACF spray parameters also affect the film formation regardless of the cutting tool geometry used. In general, the area-averaged film thickness and velocity in the tool-chip contact region are found to increase with increasing fluid flow rate. Increasing gas pressure results in reduction of the film thickness and an increase in the film velocity.
(3) Film thickness and velocity are found to affect the machining performance during turning of titanium alloy. For all the tool geometries considered in this study, the normalized flank wear is found to be the lowest for a certain film thickness value ($\approx 5.5\ \mu$m) and it is found to decrease with an increase in the film velocity.
(4) The sharp corner on the surface of grooved insert 1 results in the formation of a film with the desirable characteristics in the range of spray parameters considered, and hence, grooved insert 1 shows the minimum normalized flank wear compared to the other two insert geometries.

Funding Data

- National Science Foundation (Grant No. NSF-CMMI-12-33944).

References

[1] Ezugwu, E., and Wang, Z., 1997, "Titanium Alloys and Their Machinabilitya Review," J. Mater. Process. Technol., **68**(3), pp. 262–274.
[2] Ezugwu, E., Da Silva, R., Bonney, J., and Machado, A., 2005, "Evaluation of the Performance of Cbn Tools When Turning Ti–6Al–4V Alloy With High Pressure Coolant Supplies," Int. J. Mach. Tools Manuf., **45**(9), pp. 1009–1014.
[3] Nandy, A., Gowrishankar, M., and Paul, S., 2009, "Some Studies on High-Pressure Cooling in Turning of Ti–6Al–4V," Int. J. Mach. Tools Manuf., **49**(2), pp. 182–198.
[4] Cai, X. J., Liu, Z. Q., Chen, M., and An, Q. L., 2012, "An Experimental Investigation on Effects of Minimum Quantity Lubrication Oil Supply Rate in High-Speed End Milling of Ti–6Al–4V," Proc. Inst. Mech. Eng., Part B, **226**(11), pp. 1784–1792.
[5] Nath, C., Kapoor, S. G., DeVor, R. E., Srivastava, A. K., and Iverson, J., 2012, "Design and Evaluation of an Atomization-Based Cutting Fluid Spray System in Turning of Titanium Alloy," J. Manuf. Processes, **14**(4), pp. 452–459.
[6] Hoyne, A. C., Nath, C., and Kapoor, S. G., 2013, "Characterization of Fluid Film Produced by an Atomization-Based Cutting Fluid Spray System During Machining," ASME J. Manuf. Sci. Eng., **135**(5), p. 051006.
[7] Ghai, I., 2010, "Analysis of Droplet Behavior on a Rotating Surface in Atomization-Based Cutting Fluid Systems for Micro-Machining," Ph.D. thesis, University of Illinois at Urbana-Champaign, Champaign, IL.

[8] Ganguli, S., and Kapoor, S. G., 2016, "Improving the Performance of Milling of Titanium Alloys Using the Atomization-Based Cutting Fluid Application System," J. Manuf. Processes, **23**, pp. 29–36.
[9] Friedrich, M. A., Lan, H., Wegener, J., Drallmeier, J., and Armaly, B. F., 2008, "A Separation Criterion With Experimental Validation for Shear-Driven Films in Separated Flows," ASME J. Fluids Eng., **130**(5), p. 051301.
[10] Baxter, S., Power, H., Cliffe, K., and Hibberd, S., 2009, "Three-Dimensional Thin Film Flow Over and Around an Obstacle on an Inclined Plane," Phys. Fluids, **21**(3), p. 032102.
[11] Nath, C., Kapoor, S. G., Srivastava, A. K., and Iverson, J., 2013, "Effect of Fluid Concentration in Titanium Machining With an Atomization-Based Cutting Fluid (ACF) Spray System," J. Manuf. Processes, **15**(4), pp. 419–425.
[12] Tanveer, A., Marla, D., and Kapoor, S. G., 2016, "A Thermal Model to Predict Tool Temperature in Machining of Ti-6Al-4V Alloy With an Atomization-Based Cutting Fluid Spray System," ASME Paper No. MSEC2016-8595.
[13] Pattabhiraman, A., Marla, D., and Kapoor, S. G., 2016, "A Computational Model to Study Film Formation and Debris Flushing Phenomena in Spray-Electric Discharge Machining," ASME J. Micro Nano-Manuf., **4**(3), p. 031002.
[14] ANSYS, 2011, "Ansys Fluent 14.0: Theory Guide," Ansys, Inc., Canonsburg, PA.
[15] Sonics & Materials, 2017, "Product Literature/Manuals," Sonics & Materials, Newtown, CT, accessed June 28, 2017, https://www.sonics.com/liquid-processing/resources/product-literature-manuals/
[16] Kim, J.-D., and Kweun, O.-B., 1997, "A Chip-Breaking System for Mild Steel in Turning," Int. J. Mach. Tools Manuf., **37**(5), pp. 607–617.
[17] Zhou, L., 2001, "Machining Chip-Breaking Prediction With Grooved Inserts in Steel Turning," Ph.D. thesis, Worcester Polytechnic Institute, Worcester, MA.
[18] Kennametal, 2017, "Product Selector," Kennametal, Latrobe, PA, accessed June 28, 2017, https://www.kennametal.com/en/resources/product-selector.html